Nonvolatile floating gate memory containing AgInSbTe–SiO_2 nanocomposite layer and capping the HfO_2/SiO_2 composite blocking oxide layer

2012 Nanotechnology 23 225703

(http://iopscience.iop.org/0957-4484/23/22/225703)

Nanotechnology **23** (2012) 225703 (8pp) doi:10.1088/0957-4484/23/22/225703

Nonvolatile floating gate memory containing AgInSbTe–SiO_2 nanocomposite layer and capping the HfO_2/SiO_2 composite blocking oxide layer

Kuo-Chang Chiang and Tsung-Eong Hsieh

Department of Materials Science and Engineering, National Chiao Tung University, 1001 Ta-Hsueh Road, Hsinchu 30010, Taiwan, Republic of China

E-mail: tehsieh@mail.nctu.edu.tw

Received 12 January 2012, in final form 3 April 2012
Published 10 May 2012
Online at stacks.iop.org/Nano/23/225703

Abstract

An extremely large memory window shift of about 30.7 V and high charge storage density = 2.3×10^{13} cm^{-2} at ±23 V gate voltage sweep were achieved in the nonvolatile floating gate memory (NFGM) device containing the AgInSbTe (AIST)–SiO_2 nanocomposite as the charge trap layer and HfO_2/SiO_2 as the blocking oxide layer. Due to the deep trap sites formed by high-density AIST nanocrystals (NCs) in the nanocomposite matrix and the high-barrier-height feature of the composite blocking oxide layer, a good retention property of the device with a charge loss of about 16.1% at ±15 V gate voltage stress for 10^4 s at the test temperature of 85 °C was observed. In addition to inhibiting the Hf diffusion into the programming layer, incorporation of the SiO_2 layer prepared by plasma-enhanced chemical vapor deposition in the sample provided a good Coulomb blockade effect and allowed significant charge storage in AIST NCs. Analytical results demonstrated the feasibility of an AIST-SiO_2 nanocomposite layer in memory device fabrication with a simplified processing method and post-annealing at a comparatively low temperature of 400 °C in comparison with previous NC-based NFGM studies.

(Some figures may appear in colour only in the online journal)

1. Introduction

Nonvolatile floating gate memory (NFGM) is the key component of portable electronic products in the present day. With the progress of device scale-down and demand of high storage capacity, relevant studies have been performed in order to overcome the difficulties encountered in conventional memory devices containing poly-silicon (poly-Si) as the programming layer [1–3]. Recently, NFGM devices utilizing either semiconductor or metallic nanocrystals (NCs) as the discrete charge storage traps have attracted considerable attention due to their advantages of low lateral leakage current, low power consumption, high operative efficiency and better endurance [4–6]. Tiwari *et al* first implanted the Si NCs in NFGM [7] and, afterwards, various NFGMs containing semiconductor NCs such as germanium (Ge) [8] and SiGe [9] or transition metal NCs such as silver (Ag) [1], ruthenium (Ru) [10], tungsten (W) [11], cobalt (Co) [12], platinum (Pt) [13], gold (Au) [14], nickel (Ni) [15], molybdenum (Mo) [16], chromium (Cr) [17] and iridium (Ir) [18] were reported. Among these, the transition metal NCs provided better memory performance and retention characteristics due to their high thermal stability and suitable physical properties [10–18]. The maximum memory window (ΔV_{FB}) shift = 15 V at ±17 V gate voltage sweep was achieved in NFGM by containing Cr NCs as the charge storage traps [17]. However, complicated processing methods such as pulsed-laser deposition (PLD) [3], atomic layer

deposition (ALD) [10] and ion implantation [15] are usually required to deposit the thin metal layers for subsequent NC formation. Another difficulty encountered in NC-based NFGMs is that post-annealing at relatively high temperatures (above 600 °C) is usually required to accomplish high-density NCs with uniform dispersion. Inadequate thermal processing might cause either oxidization of NCs or the interdiffusion in between NCs and the surrounding oxide, leading to the degradation of charge-capture efficiency of NCs [19]. Moreover, the charge trapping layers have to be capped by appropriate dielectric layers in order to reduce the leakage current and alleviate the charge injection in between the gate and programming layer for reliable data retention in NC-based NFGM [20]. HfO_2 is the most promising material for such purposes due to its relatively high dielectric constant ($k = 25$) and large bandgap ($E_g = 5.68$ eV) properties [21]. Nevertheless, the relatively low recrystallization temperature (about 500 °C) and high oxygen diffusivity of HfO_2 might lead to high leakage current and poor device performance [21–23]. Nitrogen (N_2) [22] or alumina (Al_2O_3) [23] have been incorporated in HfO_2 to eliminate those deficiencies; however, it might interrupt the stoichiometry of the deposited layer and escalate the complication of fabrication processes.

Chalcogenides are well-known recording media for optical data storage due to their ultrafast phase-transition rates and comparatively low recrystallization temperatures [24]. When the chalcogenides are implanted in NCs, these unique characteristics enable a low-temperature post-annealing with short time duration that may suppress the undesired oxidation and interdiffusion mentioned previously. Moreover, chalcogenides possess the E_g and electron affinities similar to those of Si and their charge trapping effects are suitable for NFGM applications [25]. The feasibility of chalcogenides to NFGM has been demonstrated by the study which reports the ΔV_{FB} shift = 6.6 V at ±8 V gate voltage sweep and charge storage density = 5.2×10^{12} cm^{-2} in the device containing a sole AgInSbTe (AIST)–SiO_2 nanocomposite programming layer [26]. In this study, the AIST-SiO_2 nanocomposite-based NFGM capped by the HfO_2/SiO_2 composite blocking oxide layer is prepared and the correlations of electrical performance to microstructures of such a memory device are evaluated accordingly. In particular, the effects of barrier-height configuration on the charge trapping and transport behaviors of samples are discussed in terms of the analytical results presented as follows.

2. Experiments

Figure 1 schematically illustrates the NFGM device structure prepared in this study. Such a metal–insulator–semiconductor (MIS) structure was fabricated on p-type Si(100) substrates (resistivity = 1–20 Ω cm) pre-cleaned by a standard RCA process and immersed in a diluted HF solution to remove native oxides. First, the AIST (doped Sb_2Te alloy with a stoichiometry of $Ag_{0.1}In_{0.2}Sb_2Te$ supplied by Solar Applied Materials Technology Co., Taiwan, ROC) powder was pressed into disc pellets 12 mm in diameter.

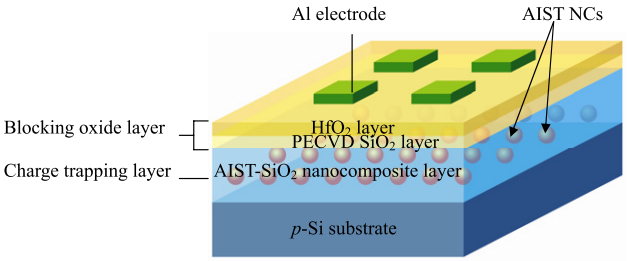

Figure 1. Schematic illustration of NFGM device structure.

After mounting an appropriate number of AIST pellets on a 3 inch quartz sputtering target, the deposition of the AIST-SiO_2 nanocomposite layer was carried out in a vacuum system with background pressure better than 2×10^{-6} Torr. About a 30 nm thick AIST-SiO_2 nanocomposite layer was deposited on the Si substrate via the target-attachment sputtering method [26, 27] under the conditions of working pressure = 3 mTorr, rf gun power = 100 W and argon (Ar)/N_2 inlet gas flow ratio = 10:2 (in units of sccm). The purpose of N_2 incorporation during sputtering is to suppress the oxygen defects in the nanocomposite layer [28] and enhance the surface polarization effect [29] so as to improve the leakage current property. Subsequently, the HfO_2/SiO_2 /AIST-SiO_2 NFGM sample was prepared by depositing a 7 nm thick PECVD SiO_2 layer on the AIST-SiO_2 nanocomposite layer using tetraethoxysilane (TEOS) as the precursor at a temperature of 250 °C followed by the sputtering deposition of a 7 nm thick HfO_2 layer at working pressure = 3 mTorr, rf gun power = 100 W and Ar inlet gas flow = 10 sccm. Afterwards, the sample was annealed by using an infrared convey furnace at 400 °C for 90 s in atmospheric ambient in order to induce the recrystallization of the AIST phase in the nanocomposite layer. Finally, a 300 nm thick aluminum (Al) electrode 0.2 mm in diameter was deposited by e-beam evaporation to complete the sample preparation. Notably, the post-annealing condition delineated above has been optimized for achieving the best device performance. It was found that inadequate annealing would cause either insufficient recrystallization or excessive oxidation of the AIST phase, leading to undesired NFGM properties.

Transmission electron microscopy (TEM, FEI TECNAI G2 F20 S-TWIN) equipped with an energy dispersive spectroscopy (EDX, Link ISIS 300) was adopted to characterize the microstructures of the NFGM samples. Evolutions of composition and chemical status of elements in nanocomposite layers were analyzed by an x-ray photoelectron spectroscopy (XPS, PHI Quantera SXM). Capacitance–voltage (C–V) and charge retention properties of NFGM devices were evaluated by an HP 4284A precision LCR meter at a frequency of 1 MHz. The current–voltage (I–V) profiles were measured by an HP 4156B semiconductor parameter analyzer in conjunction with a probe tester (SANWA, WM-365A-1) in order to explore the conduction mechanisms of the sample.

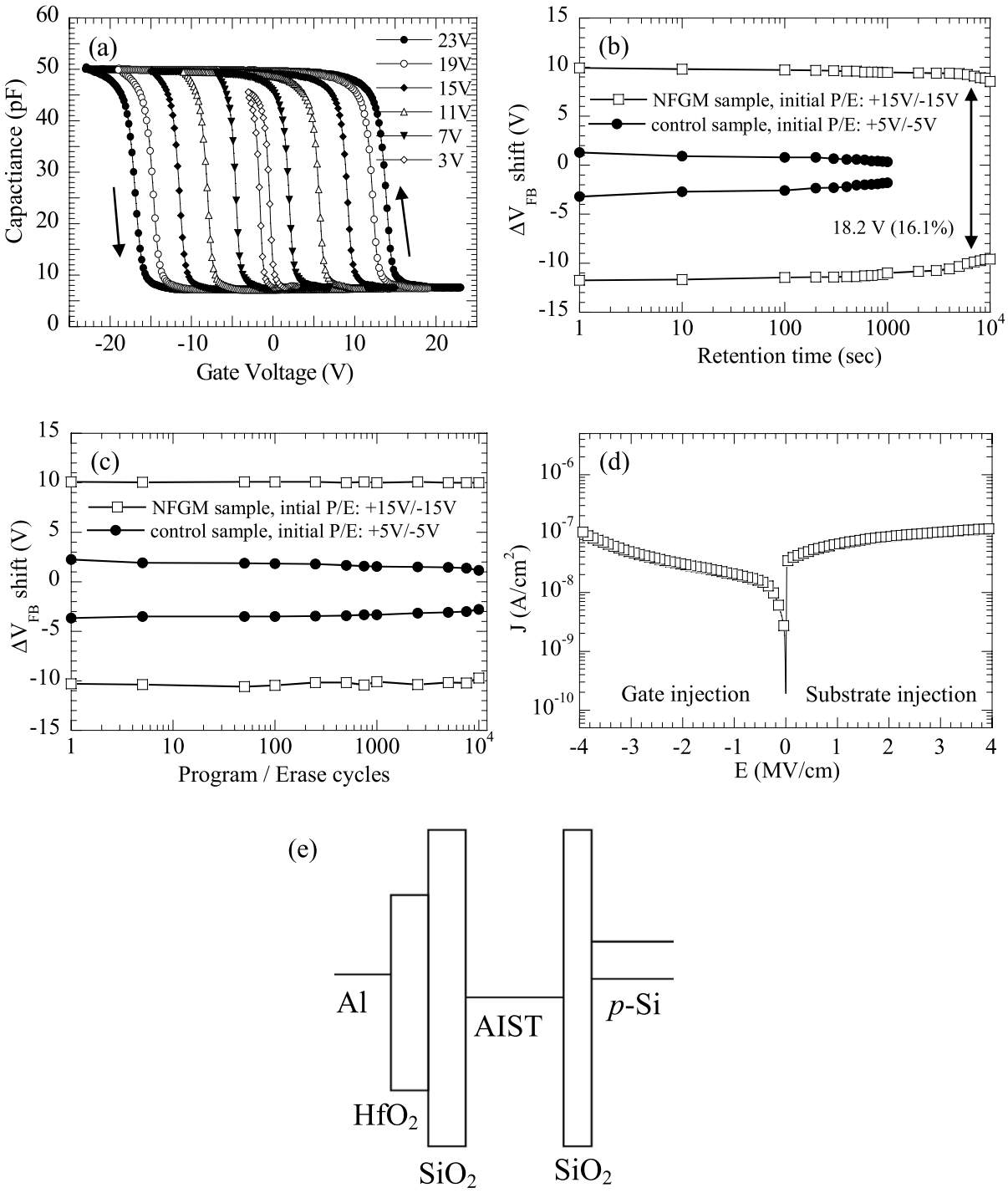

Figure 2. (a) *C–V* profiles for the NFGM device subjected to gate voltage sweep ranging from ±3 to ±23 V. (b) Charge retention characteristics at 85 °C and (c) endurance characteristics of NFGM and controlled samples subjected to ±15 V and ±5 V gate voltage stress, respectively. (d) *J–E* profiles and (e) schematic illustration of band diagram for NFGM sample.

3. Results and discussions

Figure 2(a) shows the *C–V* profiles of the NFGM sample subjected to the gate voltage sweep ranging from ±3 to ±23 V. A counterclockwise hysteresis with extremely large ΔV_{FB} shift = 30.7 V at ±23 V voltage sweep can be readily seen, implying the saturated substrate injection of charges into the AIST NCs which serve as the charge storage traps. The counterclockwise hysteresis is known to correlate with the electron transport mechanism [5]. Namely, by applying the positive bias on the gate to form the program state, the electrons injected from the Si substrate would be trapped in the AIST NCs. An increase of bias is required for further incoming electrons to overcome the repulsive electric field built by the trapped electrons, consequently resulting in the positive ΔV_{FB} shift. On the other hand, when a negative

bias is applied on the gate to form the erase state, the electrons would escape from the AIST NCs to the Si substrate. Sufficiently high bias would be required to remove the charges trapped in AIST NCs and hence induce the negative ΔV_{FB} shift. The maximum charge storage density was found to be 2.3×10^{13} cm^{-2} according to the formula [23], $N = (C_{acc}\Delta V_{FB})/(qA)$, where C_{acc} is the accumulation capacitance, q is the electron charge and A is the electrode area. In comparison with the C–V properties of NFGM containing a sole AIST-SiO_2 nanocomposite layer [26], the capping of the HfO_2/SiO_2 composite blocking oxide layer indeed improved the electrical performance of the NFGM device.

The highly symmetrical ΔV_{FB} shifts reveal an equilibrium of saturated electron trapping and hole trapping in the AIST NCs with excellent charge retention during the forward and reverse bias sweeps in the NFGM sample. In particular, the enlargement of ΔV_{FB} shift in the positive bias side indicates an increase of electron storage in AIST NCs under positive bias [13]. Our experiment also observed that the electrical properties of the NFGM sample barely changes with storage time whereas that of the sole-layer AIST-SiO_2 NFGM device degrades moderately with the increase of sample storage time. It is believed that the PECVD SiO_2 layer may effectively passivate the device and terminate the environmental attacks. The enhancement of charge-capture efficiency in the sample will be discussed in terms of the microstructure and composition analyses presented as follows.

In order to illustrate the operational reliability of the NFGM sample, the charge retention and endurance characteristics were investigated and compared with the measured results of the sample without the HfO_2/SiO_2 composite blocking oxide layer (i.e. the controlled device containing a sole AIST-SiO_2 nanocomposite layer). Figure 2(b) presents the charge retention characteristics of the NFGM samples in which the ΔV_{FB} shifts subjected to alternating electron (program) and hole (erase) injections were measured up to 10^4 s under the gate voltage stress for 10 s. We note that severe deterioration of the ΔV_{FB} shift is observed in the controlled sample when gate voltage stress exceeds ± 8 V. As a result, the gate voltage stress conditions varied for various samples, i.e. the NFGMs with the HfO_2/SiO_2 capping layer were measured at ± 15 V voltage stress whereas the controlled sample without the HfO_2/SiO_2 capping layer was measured at ± 5 V voltage stress. At the test temperature of 85 °C, a large ΔV_{FB} shift of about 18.2 V and the charge loss of about 16.1% were observed in the NFGM sample capped by the HfO_2/SiO_2 oxide layer. As to the controlled sample, it exhibited poor device durability since the retention property diminished after 10^3 s. The large amount of charges sustained for data storage is attributed to the deep trap sites in the AIST-SiO_2 nanocomposite layer, which suppress the direct tunneling from the trapping layer into the substrate [30]. In addition, it is known that the increase of the ΔV_{FB} shift is correlated to the reduction of charge injection from the gate through the blocking oxides [31] and a high-quality blocking oxide layer with appropriate thickness is essential to the satisfied charge storage capability of the NFGM [17].

Figure 2(c) depicts the endurance characteristics of NFGM samples, with and without the HfO_2/SiO_2 capping layer, measured at the pulse gate voltage stress of ± 15 V and ± 5 V for 10 ms duration, respectively. For the sample containing HfO_2/SiO_2 capping layer, the ΔV_{FB} shift remained stable without significant decay after 10^4 pulse cycle operations. This is ascribed to the high-barrier feature of the HfO_2/SiO_2 oxide layer which effectively inhibits the injection of charge trapped in AIST NCs to the gate electrode so as to yield a stable ΔV_{FB} shift property during the cycle operation. In comparison with previous studies utilizing at least 20 nm thick blocking oxide layers [12–19], the HfO_2/SiO_2 composite oxide layer with thickness less than 15 nm is able to suppress the charge injection in the NFGM and implies the good retention property. This is ascribed to the insertion of a PECVD SiO_2 layer with relatively large E_g (=9 eV) which renders a sufficiently high barrier to alleviate the charge tunneling.

Figure 2(d) presents the profiles of leakage current density versus applied bias field (J–E) of NFGM samples deduced by the I–V measurement. A relatively low leakage current and highly symmetrical J–E profile can be readily seen. The symmetry in the J–E profiles resulted from the similarity in material properties and conduction mechanisms across the Al gate/nanocomposite and nanocomposite/Si substrate interfaces [32–34]. This is illustrated by the plot of band diagrams for the sample in the cases of gate and substrate injections depicted in figure 2(e). We note that the presence of material species in figure 2(e) is plotted in accord with the results of TEM and XPS analyses. As shown in this plot, the charge trapping layer is, in fact, enclosed in between two SiO_2 layers and thus a symmetrical J–E profile could be achieved. Moreover, the high-barrier-height PECVD SiO_2 layer in the composite blocking oxide layer is able to suppress the charge injection from the gate to AIST NCs. It consequently enhances the Coulomb blockade effect and drastically reduces the leakage current density of the sample to a value as low as 150 nA cm^{-2} in the gate injection case. As revealed by subsequent XPS analysis, the low leakage current property is also ascribed to the strong surface polarization effect [29] at the AIST/SiO_2 interface induced by the N_2 gas incorporation during sputtering.

Bersuker *et al* reported the escalation of oxygen vacancy concentration in the underlying SiO_2 matrix due to the interdiffusion of HfO_2 [35]. When the oxygen deficiency occurs in the vicinity of the Si substrate, the reduction of effective barrier height of the SiO_2 layer would promote the charge injection. Such deterioration was nevertheless inhibited by the insertion of a PECVD SiO_2 layer in our NFGM sample and, with the high-barrier-height feature of SiO_2, a leakage current property could thus be achieved.

The conduction mechanisms of NFGM samples were analyzed by the linear curve fittings of J–E data and the results are shown in figure 3 which indicates a similar conduction mechanism for the sample in the cases of substrate injection (figure 3(a)) and gate injection (figure 3(b)). The Schottky emission was found to dominate at low applied bias whereas the transport mechanism switches to space–charge-limited

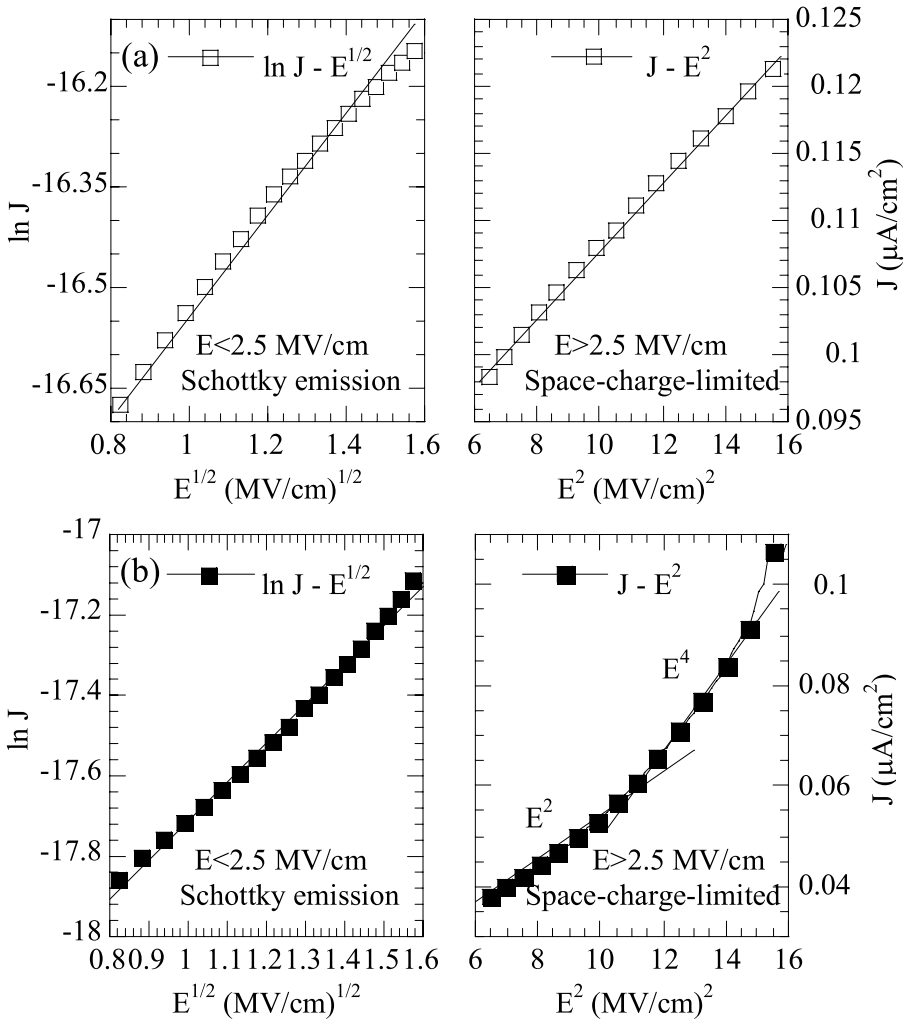

Figure 3. Conduction mechanisms deduced by the linear curve fitting results of the sample in the cases of (a) substrate injection (positive bias on Al electrode) and (b) gate injection (negative bias on Al electrode).

conduction (SCLC) at high applied bias [10]. Moreover, the same threshold field (E_{th}) = 2.5 MV cm^{-1} was found for the sample in the substrate injection and gate injection cases. This is in agreement with its symmetrical *J*–*E* profile shown in figure 2(d) and the similar barrier heights for charges tunneling under forward bias and reverse bias as depicted in figure 2(e).

Moreover, the linear curve fitting analysis observed a switch from the J–E^2 to the J–E^4 relationship for the sample in the gate injection case when the voltage bias is high. The $J \propto E^m$ power law relation indicates the SCLC characteristic with deep traps [36]. Shi *et al* suggested that the large ΔV_{FB} shift is correlated with the NCs containing sufficiently deep traps [37]. Hence, the J–E^4 relationship might indicate that the high-barrier-height HfO_2/SiO_2 oxide layer results in such a deep trap configuration in the sample and, hence, the charges stored in AIST NCs can barely tunnel back to the gate under the gate injection. It is also known that the AIST phase possesses a high work function of about 4.61 eV [38–40]. This implies a deep potential wall for efficient charge retention and a sufficient amount of charges could thus be trapped in AIST NCs [10, 41].

A cross-sectional TEM micrograph of the NFGM sample is presented in figure 4(a). A large amount of AIST NCs with sizes of about 4–6 nm can be observed in the samples as illustrated by the enlarged image shown in figure 4(b). Previous studies demonstrated that the nanocomposite layers containing uniformly dispersed AIST NCs can be prepared via the target-attachment sputtering process [26, 27] or the composite target sputtering method [42]. In comparison with other NC-based NFGM systems utilizing complicated methods for the charge trapping layer fabrication [10–19], it would be a great advantage for chalcogenide nanocomposites applied to NFGM since the high-density charge trapping layer can be easily prepared via a one-step, conventional sputtering process.

TEM characterization also revealed an about 3 nm thick SiO_2 layer lying in between the nanocomposite layer and the Si substrate as illustrated by the enlarged micrograph in figure 4(b). It might result from the interactions of the Si substrate with the oxygen atoms diffusing through the oxide matrix of the nanocomposite layer [43]. Such a SiO_2 layer formed in the sample in an inherent manner and might serve well as the tunneling layer during charge injections. Note that

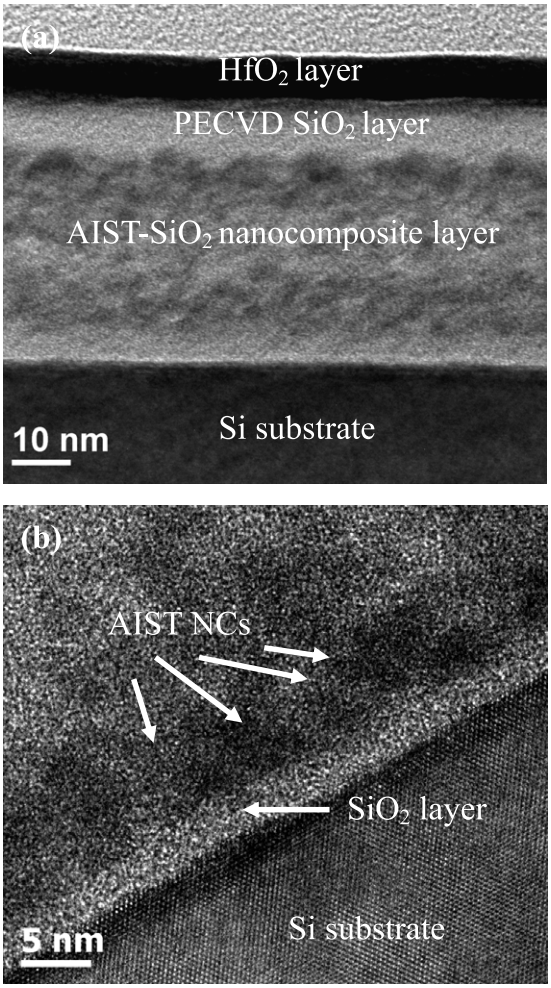

Figure 4. (a) Cross-sectional TEM micrographs of NFGM sample. An enlargement of (a) at the nanocomposite layer/Si substrate interface is shown in (b).

we also prepared the NFGM device using the Si substrate intentionally coated with a thin SiO_2 layer grown by the dry oxidization process; however, its electrical performance is similar to the results presented above. No additional deposition process for the tunneling oxide layer would be another advantage of chalcogenide nanocomposites applied to NFGM.

The Si 2p and Sb 4d XPS spectra and corresponding deconvoluted profiles obtained by the Gaussian curve fitting method [44] for the samples are separately presented in figures 5(a) and (b). Prior to the XPS analysis, the blocking oxide layer and an about 30 nm thick nanocomposite layer were removed by *in situ* Ar ion sputtering in order to expose the region enriched with AIST NCs. As shown by the Si 2p XPS spectra of figure 5(a), the SiO_x component is low while the SiO_2 component is high in the interior of the nanocomposite layer. The decrease of the SiO_x component is in agreement with the enhanced NFGM performance of the sample since the suboxide component is known to correlate with the oxide defects which led to the interface traps and insufficient barrier height during programming duration. Suppression of oxygen defects in the nanocomposite layer by inserting the PECVD SiO_2 layer to inhibit the interdiffusion of HfO_2 as well as an extra annealing provided by the 250 °C-heating process of PECVD should be responsible for the decrease of SiO_x in the sample. Moreover, the Si 2p XPS spectra revealed the presence of a Si–N bond (Si_3N_4; 101.8 eV) in the samples. This resulted from the introduction of N_2 flow during sputtering and the formation of nitride bonds in the nanocomposite layer might induce the carrier-trapping configuration and strong surface polarization at the AIST NC/matrix interfaces to impede the carrier hopping process [29], leading to the suppression of leakage current in the samples.

As shown by the Sb 4d XPS spectra in figure 5(b), the metallic Sb bonding (32.57 eV) and Sb/Si complex (33.4 eV) are simultaneously present in the nanocomposite layer. The negligible amount of antimony oxides, e.g. Sb_2O_3 and Sb_2O_5, in the sample indicates the thermal processes employed in this study do not cause severe oxidization in AIST NCs so that a satisfied charge trapping capability could be preserved. This benefit is ascribed to the ultrafast phase-change property of chalcogenides as mentioned previously. Te $3d_{5/2}$ XPS depth profiles shown in figure 5(c) reveal the Te element in the nanocomposite layer remains in metallic form (metallic Te; 573 eV), implying the charge trapping capability is mainly correlated to the AIST NCs without the disturbance caused by the oxide phases and dopants in the AIST phase. The Te $3d_{5/2}$ XPS depth profiles also reveal the presence of a small amount of TeO_2 in the nanocomposite layer. Such an oxide phase resulted from the oxidization of the AIST phase when the nanocomposite layer was exposed to air atmosphere during the transfer of the sample from the sputtering chamber to the PECVD system. Interestingly, the reduction of TeO_2 to metallic Te seemed to occur during subsequent thermal processing of PECVD since the amount of TeO_2 in the sample was comparatively less than that observed in the sample containing a sole AIST-SiO_2 nanocomposite layer [26]. This promotes the metallic content of AIST NCs in the nanocomposite layer and enhances the charge trapping capability of the NFGM sample.

The Hf 4f XPS depth profiles of the sample are presented in figure 5(d) in which the doublet in the Hf 4f XPS spectra is attributed to the Hf $4f_{7/2}$ and Hf $4f_{5/2}$ peaks [45]. Though the PECVD SiO_2 layer might react with HfO_2 to form the $HfSiO_x$ phase in the sample, as revealed by figure 5(d), it effectively impeded the Hf diffusion into the nanocomposite layer and suppressed the oxygen-deficiency reactions. Such a high-barrier-height oxide also provided a well-defined interface to prevent the leakage current and thus enhance the NFGM performance.

4. Conclusions

This study demonstrates the enhanced performance of the NFGM containing the AIST-SiO_2 nanocomposite as the charge trapping layer and HfO_2/SiO_2 as the blocking oxide layer. In such an NFGM device, *C–V* measurement revealed an extremely large ΔV_{FB} shift of 30.7 V and charge storage density of 2.3×10^{13} cm^{-2} at ±23 V gate voltage sweep whereas the retention test at 85 °C yielded a ΔV_{FB}

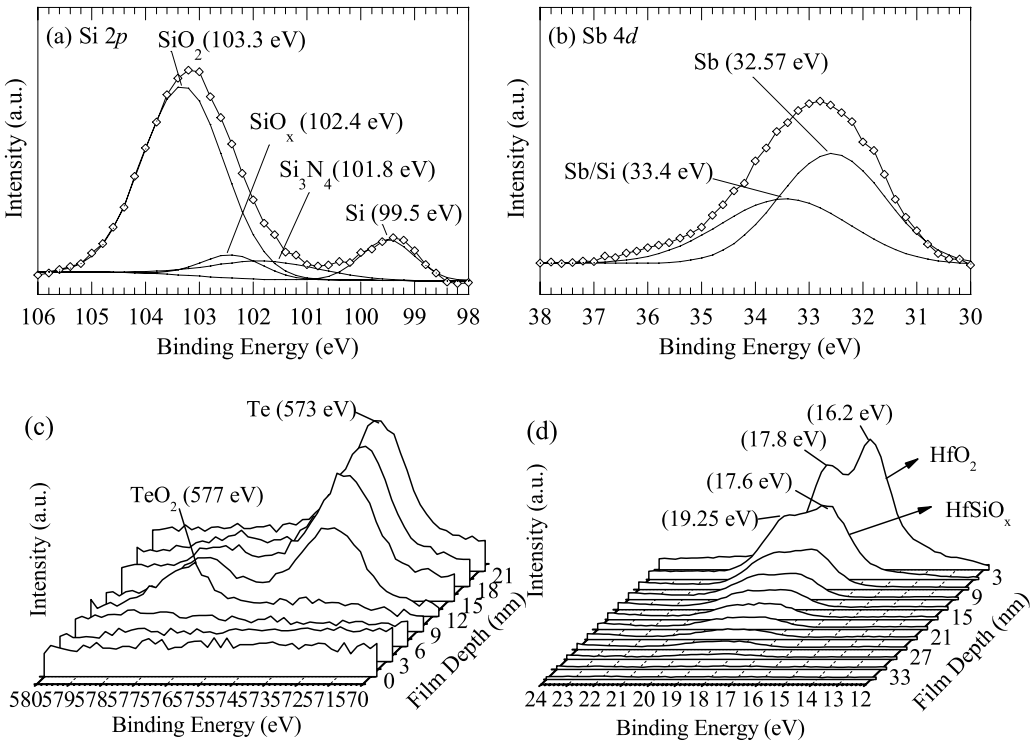

Figure 5. (a) Si 2p and (b) Sb 4d XPS spectra deduced from the interior of the nanocomposite layer of NFGM sample. The solid black curves with open diamond symbols correspond to raw XPS data while the black curves correspond to Gaussian curve fitting of raw XPS profiles. (c) Te $3d_{5/2}$ and (d) Hf 4f XPS depth profiles of the nanocomposite layer in NFGM sample.

shift of about 18.2 V and a charge loss of about 16.1% at ±15 V gate voltage stress for 10^4 s. The *I–V* test observed a symmetrical *J–E* profile with the leakage current density as low as 150 nA cm^{-2} in the cases of gate and substrate injections. Electrical analyses indicated not only an enhanced Coulomb blockade effect for significant charge storage in AIST NCs, but also similar tunneling barriers for charge transport under forward and reverse bias conditions in the NFGM sample containing the composite blocking oxide layer. TEM and XPS characterizations revealed the PECVD SiO_2 layer inserted in between the HfO_2 and nanocomposite layers and the SiO_2 layer inherently formed at the nanocomposite/Si substrate interface comprised of the symmetrical tunneling barrier configuration. The PECVD SiO_2 layer might also inhibit the interdiffusion of HfO_2 to suppress the oxygen-deficiency reactions in the matrix of the nanocomposite layer and thus improve the NFGM performance. Analytical results indicated the film quality and barrier-height feature of the blocking and tunneling layers are essential to the memory performance of NC-based NFGM. The feasibility of chalcogenide nanocomposites as the programming layer of the NFGM with satisfied memory characteristics, simplified device fabrication and low-temperature post-annealing processes is also demonstrated in this study.

Acknowledgments

This work is supported by the National Science Council (NSC), Taiwan, ROC, under contract no. NSC100-2221-E009-054-MY2. The post-annealing apparatus was supported by Gigastorage Co., TEM analysis was supported by Materials Analysis Technology Inc. and XPS analysis was supported by the Instrument Center at the National Tsing Hua University, Hsinchu, Taiwan, ROC: these are also gratefully acknowledged.

References

[1] Ryu S-W, Choi Y-K, Mo C B, Hong S H, Park P K and Kang S-W 2007 *J. Appl. Phys.* **101** 026109
[2] Choi S, Park B, Kim H, Cho K and Kim S 2006 *Semicond. Sci. Technol.* **21** 378
[3] Yuan C-L, Daramawan P, Setawan P and Lee P-S 2006 *Electrochem. Solid-State Lett.* **9** F53
[4] Tan Z, Samanta S K, Yoo W J and Lee S 2005 *Appl. Phys. Lett.* **86** 013107
[5] Lee J-S, Kim Y-M, Kwon J-H, Shin H, Sohn B-Y and Lee J 2009 *Adv. Mater.* **21** 178
[6] Dufourcq J, Mur P, Gordon M J, Minoret S, Coppard R and Baron T 2007 *Mater. Sci. Eng.* C **27** 1496
[7] Tiwari S, Rana F, Hanafi H, Hartstein A, Crabbe E F and Chan K 1996 *Appl. Phys. Lett.* **68** 1377
[8] Duguay S, Grob J J, Slaoui A, Le Gall Y and Amann-Liess M 2005 *J. Appl. Phys. Lett.* **97** 10433
[9] Kim D-W, Kim T and Banerjee S K 2003 *IEEE Trans. Electron Devices* **50** 1823
[10] Farmer D B and Gordon R G 2007 *J. Appl. Phys.* **101** 124503
[11] Samanta S K, Yoo W J, Samudra G, Tok E S, Bera L K and Balasubramanian N 2005 *Appl. Phys. Lett.* **87** 113110
[12] Pei Y, Yin C, Nishjima M, Kojima T, Fukushima T, Tanaka T and Koyanagi M 2009 *Appl. Phys. Lett.* **95** 033118
[13] Novak S, Lee B, Yang X and Misra V 2010 *J. Electrochem. Soc.* **157** H589

[14] Mikhelashvili V, Meyler B, Yofis S, Salzman J, Garbrecht M, Cohen-Hyams T, Kaplan W D and Eisenstein G 2010 *J. Electrochem. Soc.* **157** H463
[15] Hu C-W, Chang T-C, Tu C-H, Huang Y-H, Lin C C, Chen M-C, Huang F S, Sze S M and Tseng T-Y 2010 *Electrochem. Solid-State Lett.* **13** H49
[16] Lin C-C, Chang T-C, Tu C-H, Chen W-R, Hu C-W, Sze S M, Tseng T-Y, Chen S C and Lin J Y 2008 *Appl. Phys. Lett.* **93** 222101
[17] Hong A J, Liu C-C, Wang Y, Kim J, Xiu F, Ji S, Zou J, Nealey P F and Wang K L 2010 *Nano Lett.* **10** 224
[18] Wang T-J, Chu C-L, Hsieh I-J and Tseng W-S 2010 *Appl. Phys. Lett.* **97** 143507
[19] Kim J H, Yang J P, Lee J S and Hong J P 2008 *Appl. Phys. Lett.* **92** 013512
[20] Singh P W, Bisht G, Hofmann R, Singh K, Krishna N and Mahapatra S 2008 *IEEE Electron Device Lett.* **29** 1389
[21] Mikhelashvili V, Brener R, Kreninin O, Meyler B, Shneider J and Eisenstein G 2004 *Appl. Phys. Lett.* **85** 5950
[22] Wang S J, Chai J W, Dong Y F, Feng Y P, Sutanto N, Pan J S and Huan A C H 2006 *Appl. Phys. Lett.* **88** 192103
[23] Curreem K K S, Lee P F, Wong K S, Dai J Y, Zhou M J, Wang J and Li Q 2006 *Appl. Phys. Lett.* **88** 182905
[24] Chou C-C, Hung F-Y and Lui T-S 2007 *Scr. Mater.* **56** 1107
[25] Eom T, Choi B J, Choi S, Park T J, Kim J H, Seo M, Rha S H and Hwang C S 2009 *Electrochem. Solid-State Lett.* **12** H378
[26] Chiang K-C and Hsieh T-E 2010 *Nanotechnology* **21** 425204
[27] Mai H-C and Hsieh T-E 2007 *Japan. J. Appl. Phys.* **46** 5834
[28] Umezawa N, Shirashi K, Ohno T, Watanabe H, Chikyow T, Tori K, Yamabe K, Yamada K, Kitajima H and Arikado T 2005 *Appl. Phys. Lett.* **86** 143507
[29] Peng Y-Y, Hsieh T-H and Hsu C-H 2009 *J. Nanosci. Nanotechnol.* **9** 4892
[30] Chen L-C, Wu Y-C, Lin T-C, Huang J-Y, Hung M-F, Chen J-H and Chang C Y 2010 *IEEE Electron Device Lett.* **30** 1407
[31] Wang Y Q, Chen J H, Yoo W J, Yeo Y C, Chen A and Du A Y 2005 *J. Appl. Phys.* **98** 013536
[32] Wilk G D, Wallace R M and Anthony J M 2000 *J. Appl. Phys.* **87** 484
[33] Huang A. P and Chu P K 2005 *J. Appl. Phys.* **97** 114106
[34] Puthenkovilakam R, Sawkar M and Chang J P 2005 *Appl. Phys. Lett.* **86** 202902
[35] Bersuker G *et al* 2006 *J. Appl. Phys.* **100** 094108
[36] Qi X, Dho J, Tomov R, Blamire M G and MacManus-Driscoll J L 2005 *Appl. Phys. Lett.* **86** 062903
[37] Shi Y, Saito K, Ishikuro H and Hiramoto T 1998 *J. Appl. Phys.* **84** 2358
[38] Agafonov V, Rodier N, Ceolin R, Bellissent R, Bergman C and Gaspard J P 1991 *Acta Crystallogr.* C **47** 1141
[39] Grais K I and Bastawros A M 2000 *J. Appl. Phys.* **53** 5239
[40] Zuev Y M, Lee J S, Galloy C, Park H and Kim P 2010 *Nano Lett.* **10** 3037
[41] Ma X 2008 *Nanotechnology* **19** 275706
[42] Mai H-C, Hsieh T-E, Huang S-H, Lin S S and Lee T S 2008 *Japan. J. Appl. Phys.* **47** 6029
[43] Stemmer S 2004 *J. Vac. Technol.* B **22** 791
[44] Moulder J F, Stickle W F, Sobol P E and Bombem K D 1992 *Handbook of X-ray Photoelectron Spectroscopy* 2nd edn (Eden Prairie, MN: Physical Electronics)
[45] Toyoda S, Kamada H, Kumigashira H, Oshima M, Liu G L, Liu Z and Ikeda K 2008 *Appl. Phys. Lett.* **93** 182906